4.1 THE EVOLUTION OF TOTAL LIGHTNING AND RADAR CHARACTERISTICS OF TWO MESOSCALE CONVECTIVE SYSTEMS OVER HOUSTON

Charles L. Hodapp[1], Lawrence D. Carey[*1,2], Richard E. Orville[1], and Brandon L. Ely[1]

[1]Department of Atmospheric Sciences, Texas A&M University, College Station, TX
[2]ESSC/NSSTC, University of Alabama at Huntsville, Huntsville, AL

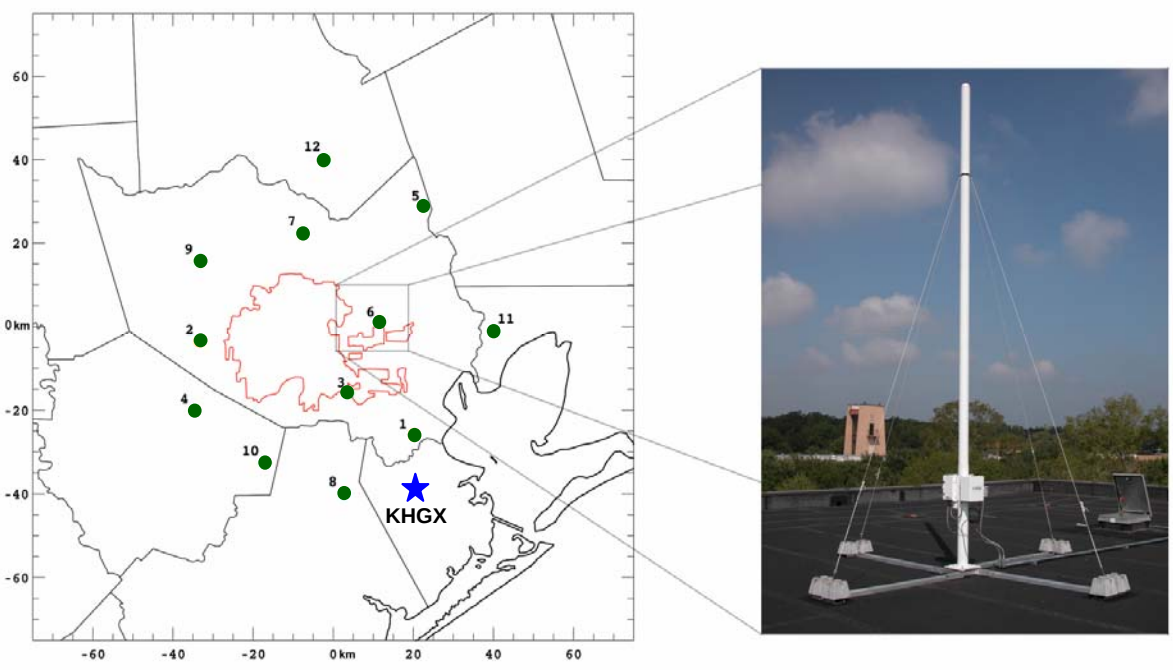

FIG.1. Locations of the 12 VHF sensors (green dots) associated with the TAMU LDAR network and the KHGX WSR-88D radar (blue star) over the Houston, Texas area. The insert is a picture of an individual LDAR II VHF sensor located on the roof of San Jacinto College in the Houston metro area.

1. Introduction

Mesoscale convective systems (MCSs) are the largest of the thunderstorms that contain regions of both convective and stratiform precipitation under one cloud complex. They may span ~ 100 km in a horizontal direction and have lifetimes of approximately 10 hours (Houze 2004). Because of their size and long lifetimes, they account for a large proportion of precipitation in both the tropics and midlatitudes. They are responsible for 30-70% of U.S. warm season rainfall (Fritch et al. 1986). MCSs often contain severe weather in the form of damaging winds, hail, and tornadoes and additionally pose a flash flooding threat (Maddox 1983, Houze et al. 1990). Not only do MCSs produce severe weather, they are also prolific producers of lightning and contain a significant fraction of warm season CG lightning in the central U.S. (Goodman and MacGorman 1986).

The lightning properties of these systems have been the focus of many research studies, with much of the past attention focusing on cloud-to-ground (CG) lightning in relation to radar or satellite inferred storm structure (e.g., Goodman and MacGorman 1986, Rutledge and MacGorman 1988, Rutledge et al. 1990). Recently however, networks capable of accurately measuring the time of arrival of impulsive VHF radiation from lightning propagation have been employed, allowing researchers to produce highly detailed pictures of the three dimensional lightning structure in storms (e.g., Goodman et al., 2005). The deployment of the Texas A&M University (TAMU) Lightning Detection and Ranging (LDAR) network in Houston, Texas, has allowed the three-dimensional properties of total (i.e., CG and

* *Corresponding author's email address*: larry.carey@nsstc.uah.edu

intracloud [IC]) lightning to be readily observed in a sub-tropical, coastal, urban environment. Two leading line trailing stratiform (LLTS) MCSs formed, evolved, and traversed the Houston LDAR network on 31 October 2005 and on 21 April 2006. The objective of this study is to document the evolution in total lightning and radar reflectivity in these two MCS cases, with emphasis on the stratiform region.

2. Data and Methodology

The Houston (KHGX) Weather Surveillance Radar – 1988 Doppler (WSR-88D) is used in conjunction with LDAR VHF lightning source data and National Lightning Detection Network (NLDN) ground flash data to provide insight into the electrical nature and lightning structure of the two MCSs as they passed within the effective range of the Houston LDAR network. The Level-II WSR-88D reflectivity data from KHGX are used to analyze the reflectivity structure of two LLTS MCSs that traversed Houston on 31 October 2005 and 21 April 2006.

The three dimensional location and time of VHF radiation sources emitted during the electrical discharge of lightning is detected by Texas A&M University's Lightning Detection and Ranging (LDAR) network which is composed of 12 sensors around the Houston metropolitan area (Fig. 1). During the time of the two cases being analyzed, 8 of the 12 sensors were fully operational. Ely et al. (2008) found that the detection efficiency of VHF sources dropped off considerably beyond a radial distance of 90-100 km from the center of the network. Because of the reduced detection efficiency, this study will only consider VHF sources that are within ~100 km from the center of the network, reflecting the network's approximate operational range. The VHF sources used in this study are located in the stratiform and convective regions along a segment of the convective line that was relatively straight for 100 (90) km for the 31 Oct. 2005 (21 Apr. 2006) event.

Flash characteristics are obtained for each region of the MCS by using a modified version of a NASA flash algorithm which groups individual VHF sources into flashes based on temporal and spatial restraints. Total flash rates are calculated for each region along with flash rates of those specific flashes originating in each region. These flash rates give clues into how electrified each MCS region is and whether or not flashes are originating in one region (e.g., convective) and propagating into another region (e.g., stratiform).

NLDN flashes with positive peak currents less than 15 kA are discarded because they could be misidentified IC flashes (Biagi et al. 2007). NLDN flash rates and characteristics are found for the defined convective and stratiform regions of the MCS. The evolution of NLDN flash characteristics such as flash rate, percent positive flashes, IC:CG ratio, are documented for each region.

The stroke level data were also acquired from Vaisala, Inc. in order to associate NLDN positive strokes with a parent LDAR detected flash. Once the NLDN flashes are paired to a parent LDAR flash, they are grouped into three categories based on location: (1) stratiform, if the location falls within the defined stratiform domain; (2) non-stratiform, if the location falls within the analysis domain, but outside the stratiform region; and (3) outside, if the flash origination falls outside the analysis domain. These groupings are then subdivided by when the flashes occurred, either before or after 2300 (1207 UTC) for the 31 Oct 2005 (21 Apr. 2006) MCS. This time was used because it appeared as a midway point for stratiform development. By determining the origin of these LDAR flashes, the locations of the initiation point of the positive CGs are determined. The mean, maximum, and minimum are computed for the LDAR flash VHF source count, along with the maximum LDAR flash extent (maximum distance between any two lightning VHF sources) and NLDN return stroke current for the +CG flashes occurring in the stratiform and non-stratiform categories.

3. Results

a) 31 October 2005 MCS

On 2005 October 31, a symmetric LLTS MCS passed within range of Houston's WSR-88D (KHGX) and Texas A&M's LDAR network. As the MCS traversed the LDAR network it underwent significant evolution in both the convective and stratiform regions. The evolution the MCS will be analyzed by using radar and total lightning characteristics during a time span of an hour and a half from 22:27 UTC to 22:53 UTC, when it was within operational range of the LDAR network.

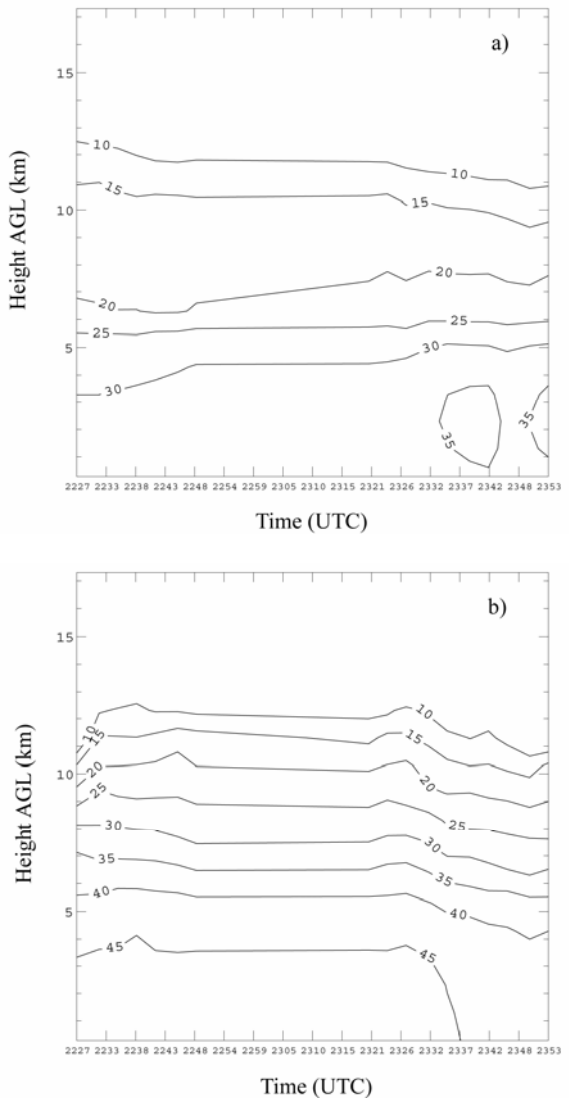

FIG.2. Time series of mean reflectivity at all elevations for the a) stratiform and b) convective regions of the 31 October MCS. Mean reflectivity is contoured every 5 dBZ from 10 dBZ to 55 dBZ.

Time series plots of mean reflectivity at all heights are shown for the stratiform (Fig. 2a) and convective (Fig. 2b) regions. Reflectivity values in the stratiform region at low-to-mid levels (< 8 km) increase steadily throughout the analysis time period. Mean reflectivity values of 20 dBZ, 25 dBZ, and 30 dBZ are found at 7 km, 5.5 km, and 3 km, respectively, at 22:27 dBZ. As the MCS matures, the mean reflectivity values of 20 dBZ, 25 dBZ, and 30 dBZ are found at higher heights of 8km, 6 km, and 5 km, respectively, at 23:53 UTC. Also, the emergence of higher reflectivity (> 35 dBZ) is found at 23:32 UTC at low levels (< 3 km). Higher reflectivity seen at low- to mid-levels as the system matures could be the result of particle growth by aggregation and deposition as they slowly sink through the mesoscale updraft toward the melting level after being ejected into the stratiform region from the rear of the convective region. The sinking motion can be illustrated by the slow decrease in low reflectivity at higher elevations (10-13 km) (Fig. 2a). Reflectivity values greater than 10 dBZ are seen near the altitude of 12.5 km initially. However, these reflectivity values are only seen below 11 km at later times. As the reflectivity at higher heights in the stratiform region of the MCS decrease, low-to-mid levels see a significant increase in reflectivity.

The convective region on the other hand, shows an increase of mean reflectivity values at most elevations until 22:38 UTC, followed by little change throughout all heights until 23:26 UTC. After 23:26 UTC, the convective region begins to decrease in intensity rapidly (Fig 2b). The increase in reflectivity initially is shown by dBZ contours shifting from lower to higher heights, indicating a possibly of strengthening updrafts. These stronger updrafts would be able to carry particles to higher levels and also able to support larger ice particle formation such as graupel and hail. As the reflectivity contours begin to sink down to lower altitudes, this could signify weakening of the updraft, causing larger ice particles to fall lower in the cloud and then to the ground.

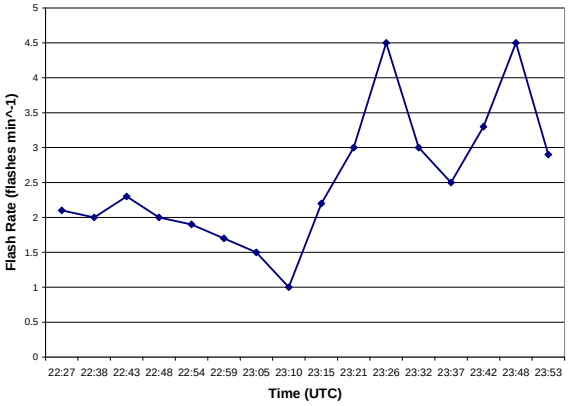

FIG.3. Time series plot of the 31 October MCS stratiform flash rate during ten minute intervals centered on the radar volume scan times.

As the stratiform region intensified total flash rates in the stratiform region doubled from 1.5-2 flashes min^{-1} to over 3-4 flashes min^{-1} during the analysis time period (Fig. 3). These stratiform flashes are

classified as to whether or not they originated in the analysis domain consisting of defined convective, transition, and stratiform regions. Throughout all times, a mean of 80% of stratiform flashes originated within the analysis domain (Fig. 4). This would indicate that few flashes propagate into the stratiform region from areas outside the analysis domain. In taking into account all flashes that originate within the analysis domain, the percentage of flashes actually originating in the stratiform region varies depending on whether the time is before or after 23:15 UTC as the stratiform region begins to intensify.

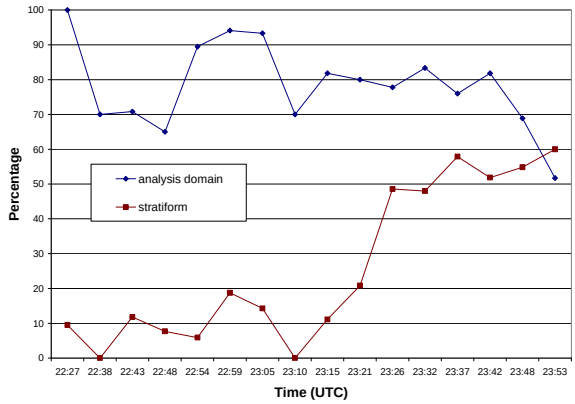

FIG.4. Time series plot of the percentage of stratiform flashes originating in the 31 October MCS analysis domain (convective, transition, or stratiform regions). Also plotted is the percentage of these flashes that originate in the stratiform region.

Before 23:15 UTC, an average of 10% of stratiform flashes originating in the analysis domain actually originated in the stratiform region. However, after 23:15 UTC, this percentage increased to over 50% (Fig. 4). The majority of stratiform flashes in the analysis domain originate in the stratiform region once the stratiform region becomes fully developed.

In conjunction with LDAR data, NLDN data is used to document important trends in CG flashes during the evolution of the MCS. The IC:CG ratio for the stratiform region remains fairly constant (~4) throughout the time period (Fig. 5). However, the total flash rate in the stratiform region shows a general increasing trend with time; which along with a steady IC:CG ratio, indicates increasing CG rates with time as well. CG flash rates are found to increase from 0.1 - 0.6 CG flashes min^{-1} before 23:15 UTC to 0.6 - 1 flashes min^{-1} after 23:15 UTC (Fig. 6). The percent of positive CGs in the stratiform region fluctuates between 25% and 50%, with higher percentages concentrated near the end of the analysis period. The increase in the NLDN flash rate in the stratiform region (Fig. 6) supports the similar increase found in the LDAR indicated flash rate (Fig. 3) during the same time period.

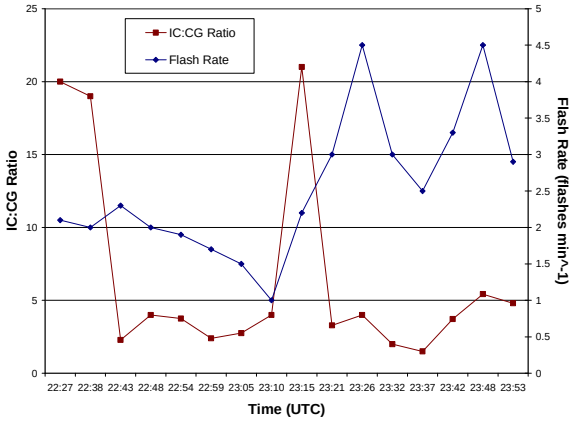

FIG.5. Time series plot of the flash rate and the IC:CG ratio in the 31 October MCS over a ten minute time span centered on the radar volume scan time.

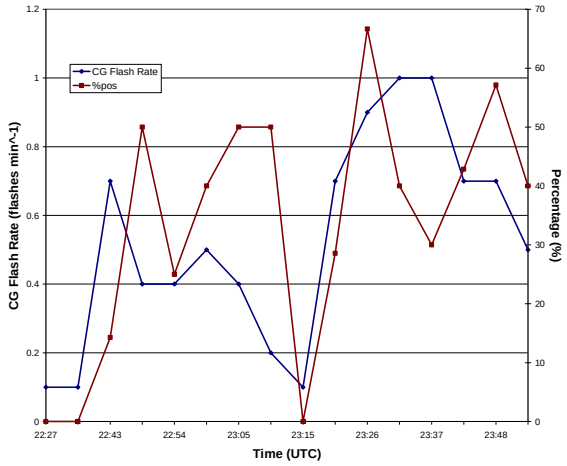

FIG.6. Time series plot of the CG flash rate and the percent of positive CGs occurring over a ten minute time period in the 31 October MCS stratiform region.

Mean peak currents of positive and negative CG flashes differ between the stratiform and convective regions. Positive CGs in the stratiform region deposit larger peak currents than their counterparts in the convective region (Fig. 7). The

stratiform peak positive currents also show an increasing trend as the stratiform region intensifies. The stratiform mean peak negative currents are much more variable (-2 to -40 kA) than the negative peak currents in the convective region (~ -15 kA).

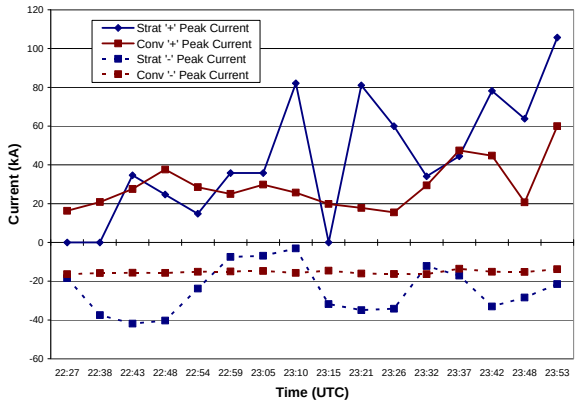

FIG.7. Time series plot of the 31 October MCS stratiform and convective CG peak currents.

Over the analysis time period, 18 separate stratiform region LDAR flashes are associated with NLDN CGs that contained a positive return stroke. Three parent stratiform flashes cannot be uniquely defined due to the lack of LDAR detected VHF sources near (< 20 km and < 1 s) the ground strike point, or multiple flashes are near the ground strike location making the association between LDAR flash and NLDN ground stroke location ambiguous.

Stratiform region positive CG strokes, which occur throughout the analysis time period, are associated with 15 unique LDAR flashes. The number of flashes originating in the stratiform, non-stratiform, and outside regions, that contain a CG with at least one positive return stroke located in the stratiform region, are 6, 5, and 4 respectively. After further subdividing the groups based on occurrence before (after) 23:15 UTC, the distributions are 0(6), 2(3), 0(4) in the stratiform, non-stratiform, and outside domains, respectively. These results, plus other positive CG flash statistics, which are taken from the NLDN and LDAR networks, are listed in Table 1.

The mean LDAR flash extent and LDAR VHF source count of flashes from the non-stratiform region are larger than those from the stratiform region, which can be expected because of the distance the flashes need to propagate in order to tap into the charge in the stratiform region (20-40 km). However, flashes originating in the stratiform region generally propagate in the along line direction and are thus limited by the line-parallel size of the domain. Larger stratiform flash extents may be seen with a larger analysis domain in the line-parallel direction. Interestingly, the mean NLDN positive peak current for flashes originating in the non-stratiform region is less than the peak current from those originating in the stratiform region, despite the shorter flash extents of the stratiform originating flashes.

Table 1: Summary of statistics for the 31 October MCS stratiform region positive CG flashes that originated in stratiform (top) and non-stratiform regions (bottom).

Stratiform			
		Count	
Total		6	
Before(after) 2315 UTC		0(6)	
	source count	**extent (km)**	**current (kA)**
mean	272	51	81
Min	20	13	12
Max	879	79	180
Non-stratiform			
		Count	
Total		5	
Before(after) 2315 UTC		2(3)	
	source count	**extent (km)**	**current (kA)**
mean	883	80	43
Min	330	48	12
Max	1986	104	82

b) 21 April 2006 MCS

On 21 April 2006, another symmetric LLTS MCS traversed within range of Houston's WSR-88D (KHGX) and Texas A&M's LDAR network. As the MCS traversed the LDAR network, it too underwent significant evolution in both the convective and stratiform regions. The evolution of the stratiform and convective regions will be analyzed by using total lightning and radar characteristics during a time span of two and a

half hours from 10:40 UTC to 13:01 UTC, when it was within operational range of the LDAR network.

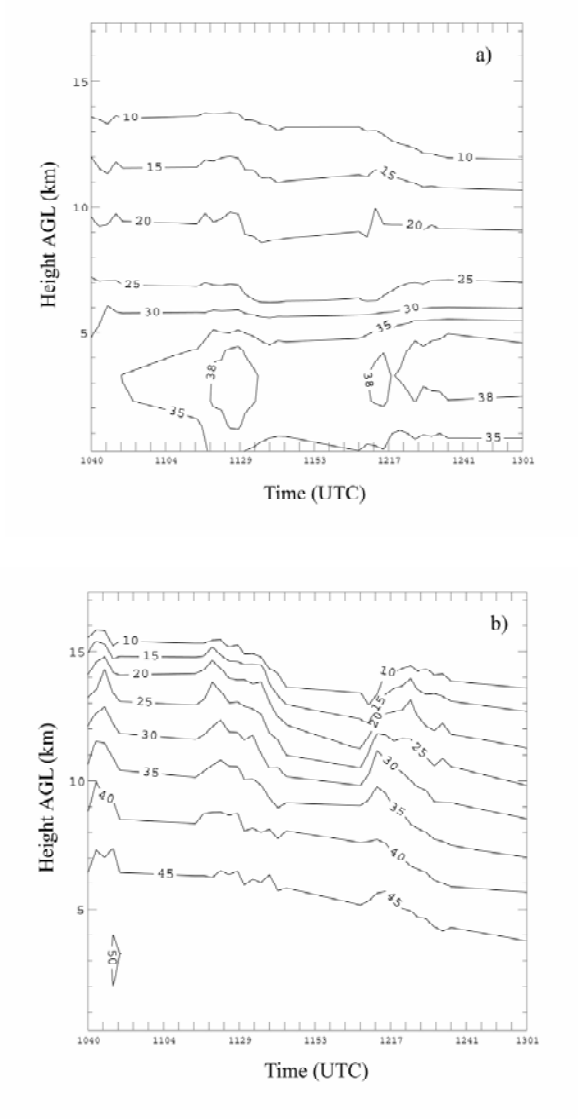

FIG.8. Time series of mean reflectivity at all elevations for the 21 April MCS a) stratiform and b) convective regions. Mean reflectivity is contoured every 5dBZ from 10 dBZ to 55 dBZ.

Once again, time series plots of mean reflectivity at all heights are shown for both the stratiform (Fig. 8a) and convective (Fig. 8b) regions. The stratiform region's greatest change throughout the time period occurs at low-to-mid levels. At heights near 4 and 5 km, reflectivity values are below 35 dBZ during early times. However, as time progresses, higher reflectivities (>35 dBZ) are seen at these heights (Fig. 3.8a). Also, reflectivities over 38 dBZ emerge at low heights (2-4 km) at later times. Higher reflectivities seen at low-to-mid levels in the stratiform region during later time periods are indicative of particle deposition, aggregation, and melting as they fall through the melting level. At higher levels (> 12 km) reflectivities fall significantly on the order of 5 dB in time (Fig. 3.8a). The mean reflectivity at 12 km is close to 15 dBZ near the beginning of the time period and falls to below 10 dBZ at the end of the analysis period. This could be the result of a combination of the convective line weakening and ejecting small ice particles at lower heights and also the particles falling from higher to lower heights in the stratiform region as time passes. During two time periods, near 11:29 UTC and 12:17 UTC, reflectivity pulses at all heights. Similar to the previous case, the stratiform region intensifies throughout the time period.

The convective region, on the other hand, shows decreasing mean reflectivity throughout all heights, similar to the 31 October MCS. Higher mean reflectivity values (> 45 dBZ) are more predominant at lower levels, with some mean

values of 50 dBZ seen during early times (Fig. 8b). At heights of 5 km and above, mean reflectivity values drop considerably. The mean reflectivity at 6 km starts above 45 dBZ and then begins to decrease down to below 40 dBZ by the end of the analysis time period. At 10 km, the mean reflectivity begins near 40 dBZ and continues to decreases significantly to below 25 dBZ. The decrease in reflectivity at mid-to-upper levels is a sign of the convective region weakening. As time passes, the weakening updraft is likely only able to support smaller particles. However, similar to the stratiform region, the reflectivity increases at all height levels near 11:29 UTC and 12:17 UTC (Fig. 8b).

Stratiform flash rates are also calculated throughout the analysis time by using a modified flash algorithm (Fig. 9). The flash rates, although noisy, increase with time from 5 flashes min^{-1} to over 10 flashes min^{-1} flashes as the stratiform region intensifies. These flashes are then classified based on their origin. The flashes were first classified as to whether or not they originated in the analysis domain consisting of the defined convective, transition, and stratiform regions. Most (70–80 %) of the electrical activity in the stratiform region originates within the analysis domain (Fig. 10). Therefore, few lightning flashes originate outside the analysis domain and propagate into the stratiform region. The percentage of flashes

that originate in the analysis domain within the stratiform region increases from near 20 % (10:40 UTC – 11:29 UTC) to as high as 60 % during later times (e.g., 12:41 UTC). The increase in the amount of flashes originating in the stratiform region occurs as the lightning pathway begins to slant downward into the region and into the melting level (not shown but similar to Ely et al. 2008).

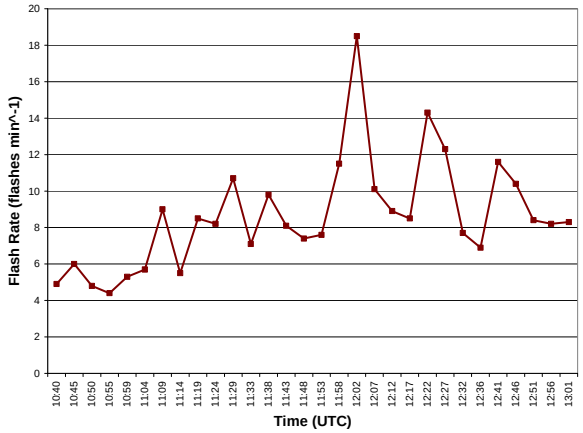

FIG.9. Time series plot of the 21 April MCS stratiform flash rate occurring over ten minute intervals centered on the radar volume scan times.

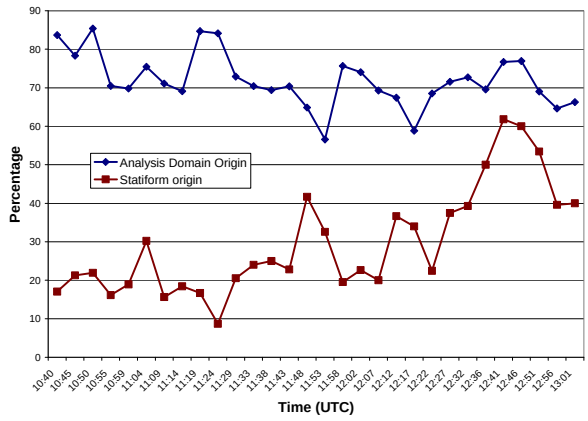

FIG.10. Time series plot of the percentage of the 21 April MCS stratiform flashes originating in the analysis domain (convective, transition, or stratiform regions). Also plotted is the percentage of these flashes that originate in the stratiform region.

NLDN data is also used to document how CG flashes evolve with the MCS. A time series plot of the total stratiform lightning flash rate and the stratiform IC:CG ratio is shown in Fig. 11. The total stratiform flash rate increases steadily as well as the stratiform CG flash rate, which is shown by the decreasing IC:CG ratio by roughly a factor of five from a maximum of ten at 11:09 UTC to a minimum of two at 13:01 UTC (Fig. 11). Figure 12 shows the stratiform CG flash rate increasing from 0.5 flashes min^{-1} to 3.4 flashes min^{-1} during the analysis time domain. As the CG flash rate increases, so does the percent of positive CG flashes. The percent of positive CG flashes during early times (1040 UTC to 1114 UTC) is $\leq$ 15%. By 1246 UTC, the percent of positive CG flashes increases to 37% (Fig. 12).

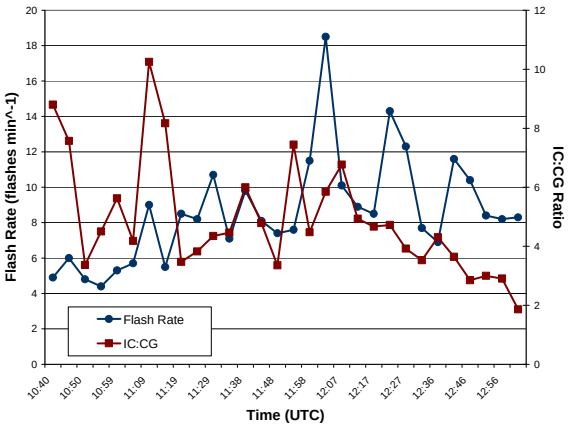

FIG.11. Time series plot of the flash rate and the IC:CG ratio in the 21 April MCS stratiform region over a ten minute time span centered on the radar volume scan time.

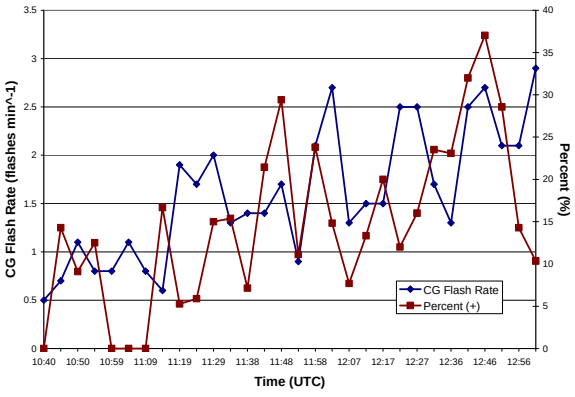

FIG.12. Time series plot of the CG flash rate and percent of positive CGs occurring over a ten minute time period in the 21 April MCS stratiform region.

The mean peak currents of stratiform and convective CG flashes also differ from one another. The stratiform peak positive currents have a tendency to be greater than the positive peak currents found in the convective region (Fig. 13). Also, the peak currents in the stratiform region increase from around 40 kA to 70 kA while the convective peak currents increase from 18 kA to 35 kA (Fig. 13). The negative peak currents in the convective region stay relatively constant near -17 kA throughout the time period. The stratiform mean negative peak currents have smaller amplitudes (~ -12 kA) than those in the convective region during the first half of the analysis time (< 11:48 UTC). However, their magnitudes increase (~ -22 kA) to surpass the convective mean peak currents in the second half of the time period (>11:48 UTC) (Fig. 13).

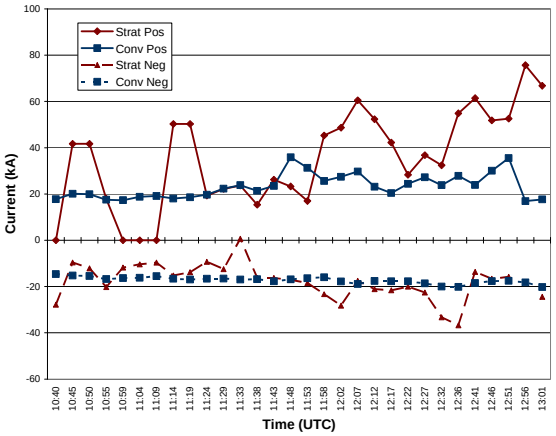

FIG.13. Time series plot of the mean stratiform and convective CG peak currents during the 21 April MCS.

Throughout the analysis time period, 36 LDAR flashes are associated with stratiform region positive CG strokes. The number of flashes originating in the stratiform, non-stratiform, and outside regions, that contain a CG with at least one positive return stroke located in the stratiform region, are 7, 19, and 10, respectively. After further subdividing the groups based on occurrence before (after) 12:07 UTC, the distributions are 2(5), 6(13), 5(5) in the stratiform, non-stratiform, and outside domains, respectively. These results, plus other positive CG flash statistics, which are taken from the NLDN and LDAR networks, are listed in Table 2.

The mean LDAR flash extent and LDAR source count of flashes from the non-stratiform region are larger than those from the stratiform region, which can be expected because of the distance the flashes need to propagate in order to tap into the charge in the stratiform region (20-40 km). However, flashes originating in the stratiform region generally propagate in the along line direction and are thus limited by the line-parallel size of the domain. Larger stratiform flash extents may be seen with a larger analysis domain in the line-parallel direction. Interestingly however, even though flashes originating in the non-stratiform domain have longer flash extents, their mean NLDN peak current is less than those that originate in the stratiform region.

Table 2. Summary of flash statistics for stratiform region positive CG flashes that originated in the 21 April MCS stratiform (top) and non-stratiform regions (bottom).

Stratiform			
		Count	
Total		7	
Before(after) 1207 UTC		2(5)	
	source count	**extent (km)**	**current (kA)**
Mean	180	49	57
Min	35	27	17
Max	460	71	112

Non-stratiform			
		Count	
Total		19	
Before(after) 1207 UTC		6(13)	
	source count	**extent (km)**	**current (kA)**
Mean	807	96	43
Min	259	50	15
Max	1679	125	111

4. Summary

MCSs are some of the largest convective systems and produce a wide variety of weather including damaging winds, hail, tornadoes, and flooding. They are also prolific producers of lightning, which is the second most fatal weather related event. This study examines the total lightning and radar reflectivity structure of two MCSs, occurring on 31 October 2005 and 21 April 2006, that traversed Houston within the effective operational range of the LDAR network in Houston, Texas. The lightning characteristics of both MCSs evolved

with intensification of their stratiform regions and weakening of their convective regions.

As the mean stratiform reflectivity increased significantly at all heights, especially near the melting level, stratiform flash rates and the percentage of flashes originating in the stratiform region increase. The total flash rates double in time and the percentage of flashes originating in the stratiform region increased from 10 - 20 % to 50 – 60% in both stratiform regions of the MCSs (Figs. 3, 4, 9, 10). Charge advection and in-situ charging (NIC melting and collisional charging) as the mesoscale updraft develops are suggested to cause enhanced charge layers and the increased electrical activity.

A majority, 19 of 26 (73%), of flashes originating in the analysis domain with a NLDN identified positive ground stroke in the stratiform region, originate in the convective or transition regions and propagate into the stratiform region before descending to the earth in the April MCS. The remaining seven positive ground flashes originate in the stratiform region. These numbers are comparable to those seen in Lang et al. (2004) and indicate that charge advection may be an important factor in positive CG production in the stratiform region of LLTS MCS. However, only 5 of 11 (45 %) flashes with a positive stroke originated from the convective region in the October MCS. Positive stratiform CG production, which is initiated in both the stratiform and convective regions, increases after 23:15 (12:07) UTC in the October (April) MCS, as radar reflectivity in the stratiform region increases. Of all the LDAR flashes associated with NDLN positive CGs, 70% occurred after 12:07 UTC in the April MCS and 82% occurred after 23:15 UTC in the October MCS (Tables 1, 2).

CGs also increase as the stratiform region intensifies. Positive CG currents found in the stratiform are generally higher than those found in the convective region and increase in time. Also, stratiform region flashes originating in the stratiform region produce higher positive CG currents than those originating in the convective region and then propagating into the stratiform and then to ground.

5. Acknowledgements

We gratefully acknowledge support from the National Science Foundation (ATM-0442011 and ATM-0321052).

6. References

Biagi, C. J, Cummins, K. L., Kehoe, K. E., Krider, E. P., 2007. National Lightning Detection Network (NLDN) performance in southern Arizona, Texas, and Oklahoma in 2003-2004. J. Geophys. Res. 112, D05208, doi:10.1029/2006JD007341.

Ely, B.L., R. E. Orville, L. D. Carey, and C. L. Hodapp, 2008: Evolution of the total lightning structure in a leading-line, trailing-stratiform mesoscale convective system over Houston, Texas. *J. Geophys. Res.*, **in press.**

Fritsch, J.M., R.J. Kane, and C.R. Chelius, 1986: The contribution of mesoscale convective weather systems to the warm-season precipitation in the United States. *J. Climate Appl. Meteor.*, **25**, 1333-1345.

Goodman, S.J., and D.R. MacGorman, 1986: Cloud-to-ground lightning activity in mesoscale convective complexes. *Mon. Wea. Rev*., **114**, 2320-2328.

--------, T. Blakeslee, H. Christian, W. Koshak, J. Bailey, J. Hall, E. McCaul, D. Buechler, C. Darden, J. Burks, T. Bradshaw, and P. Gatlin, 2005: The north Alabama lightning mapping array: Recent severe storm observations and future prospects, *Atmo. Res*., **76**, 423-437.

Houze, R.A., B.F. Smull, and P. Dodge, 1990: Mesoscale organization of springtime rainstorms in Oklahoma. *Mon. Wea. Rev*., **118**, 613-654.

Houze, R.A., 2004: Mesoscale Convective Systems. *Rev. Geophys*., **42**, RG4003, doi: 10.1029/2004RG000150.

Lang, T.J., S.A. Rutledge, and K.C. Wiens, 2004: Origins of positive cloud-to-ground lightning flashes in the stratiform region of a mesoscale convective system. *Geophys. Res. Lett*., **31**, L10105, doi:10.1029/2004GL019823.

Maddox, R.A, 1983: Large-scale meteorological conditions associated with midlatitudes mesoscale convective complexes. *Mon. Wea. Rev*., **111**, 1475-1493.

Rutledge, S.A. and D. R. MacGorman, 1988: Cloud-to-ground lightning activity in the 10-11 June 1985 mesoscale convective system observed during the Oklahoma-Kansas PRE-STORM project. *Mon. Wea. Rev.,* **116**, 1393-1408, 1988.

--------, C. Lu, and D.R. MacGorman, 1990: Positive cloud–to-ground lightning in mesoscale convective systems. *J. Atmos. Sci*., **47**, 2085-2100.